ON INFERRING EXTINCTION LAWS IN $Z \sim 6$ QUASARS AS SIGNATURES OF SUPERNOVA DUST

JENS HJORTH[1], PAUL M. VREESWIJK[2,1,3], CHRISTA GALL[4,1], AND DARACH WATSON[1]

ABSTRACT

Unusual extinction curves of high-redshift QSOs have been taken as evidence that dust is primarily produced by supernovae at high redshift. In particular, the 3000 Å Todini–Ferrara–Maiolino kink in the extinction curve of the $z = 6.20$ SDSS J1048+4637 has been attributed to supernova dust. Here we discuss the challenges in inferring robust extinction curves of high-redshift QSOs and critically assess previous claims of detection of supernova dust. In particular, we address the sensitivity to the choice of intrinsic QSO spectrum, the need for a long wavelength baseline, and the drawbacks in fitting theoretical extinction curves. In a sample of 21 QSOs at $z \sim 6$ we detect significant ultraviolet extinction using existing broad-band optical, near-infrared, and *Spitzer* photometry. The median extinction curve is consistent with a Small Magellanic Cloud curve with $A_{1450} \sim 0.7$ mag and does not exhibit any conspicuous (restframe) 2175 Å or 3000 Å features. For two QSOs, SDSS J1044−0125 at $z = 5.78$ and SDSS J1030+0524 at $z = 6.31$, we further present X-shooter spectra covering the wavelength range 0.9–2.5 μm. The resulting non-parametric extinction curves do not exhibit the 3000 Å kink. Finally, in a re-analysis of literature spectra of SDSS J1048+4637, we do not find evidence for a conspicuous kink. We conclude that the existing evidence for a 3000 Å feature is weak and that the overall dust properties at high and low redshift show no significant differences. This, however, does not preclude supernovae from dominating the dust budget at high redshift.

Keywords: accretion, accretion disks — dust, extinction — galaxies: high-redshift — quasars: general — quasars: individual (SDSS J1030+0524, SDSS J1044−0125, SDSS J1048+4637)

1. INTRODUCTION

Characterizing the properties of dust in galaxies at high redshift is important for our understanding of the physics of dust formation and its interplay with galaxy evolution. The very large dust masses found in some high-redshift QSOs from sub-mm and mm detections of their far-infrared emission (Priddey et al. 2003; Bertoldi et al. 2003; Robson et al. 2004; Priddey et al. 2008) pose a challenge to current models of the evolution of massive stars and galaxies. This is because the time since Big Bang at $z \gtrsim 6$ (< 1 Gyr) is very short for large amounts ($> 10^8$ M$_\odot$) of dust to be produced by stellar or non-stellar sources (e.g., Dwek et al. 2007; Michałowski et al. 2010a,b; Gall et al. 2011a,b,c).

Maiolino et al. (2004) observed the $z = 6.20$ QSO SDSS J1048+4637 and inferred an unusual ultraviolet (UV) extinction curve, inconsistent with known local extinction curves for the Milky Way or the Magellanic Clouds, but consistent with predictions of simple theoretical models of dust formation in supernova (SN) ejecta (Todini & Ferrara 2001; Bianchi & Schneider 2007) (for a variety of extinction curves, see Figure 1). The intriguing suggestion is that SNe are responsible for the rapid formation of dust at high redshift, whereas Asymptotic Giant Branch stars contribute significantly only at lower

redshift, when they have had time to evolve.

More recently, Gallerani et al. (2010, hereafter G10) studied a larger sample of high-redshift QSOs, including SDSS J1048+4637, and fitted their spectra with a range of theoretical SN extinction curves, assuming a QSO template spectrum (Reichard et al. 2003) with an adjustable power law slope for the underlying QSO continuum. The best-fitting extinction curves were found to be slightly more shallow than in the Small Magellanic Cloud (SMC) but no strong evidence for extinction curves of the kind suggested by Maiolino et al. (2004) was found. However, obtaining robust results from such an approach is challenging because of (i) the narrow rest wavelength range considered (~ 0.13–0.3 μm), (ii) the unknown intrinsic (unextinguished) QSO spectrum, (iii) the difficulty in estimating the continuum baseline (QSOs are dominated by broad and blended emission lines almost everywhere in their UV spectra), and (iv) the possible presence of variability, which will give rise to spurious features in the spectrum if its constituent data points were not obtained simultaneously.

While the prospects of interpreting unusual extinction curves as evidence for SN dust at high redshift are exciting, it is important to note that detecting significant extinction requires sufficiently blue intrinsic spectra of the corresponding QSOs. Indeed, previous extinction curves reported for high-redshift QSOs have required extremely blue QSOs. This would be consistent with the notion that only very blue QSOs with reddening can be detected in the first place because of the detection limit in the SDSS z' band. However, it is a concern that no QSOs at high redshift with normal intrinsic colors have been found to have extinction, especially in view of the delicate procedure of inferring an extinction curve. Moreover,

[1] Dark Cosmology Centre, Niels Bohr Institute, University of Copenhagen, Juliane Maries Vej 30, DK–2100 Copenhagen Ø, Denmark; jens@dark-cosmology.dk
[2] Department of Particle Physics and Astrophysics, Faculty of Physics, Weizmann Institute of Science, Rehovot 76100, Israel
[3] Centre for Astrophysics and Cosmology, Science Institute, University of Iceland, Dunhaga 5, IS–107 Reykjavik, Iceland
[4] NASA, Goddard Space Flight Center, 8800 Greenbelt Road, Greenbelt, MD 20771
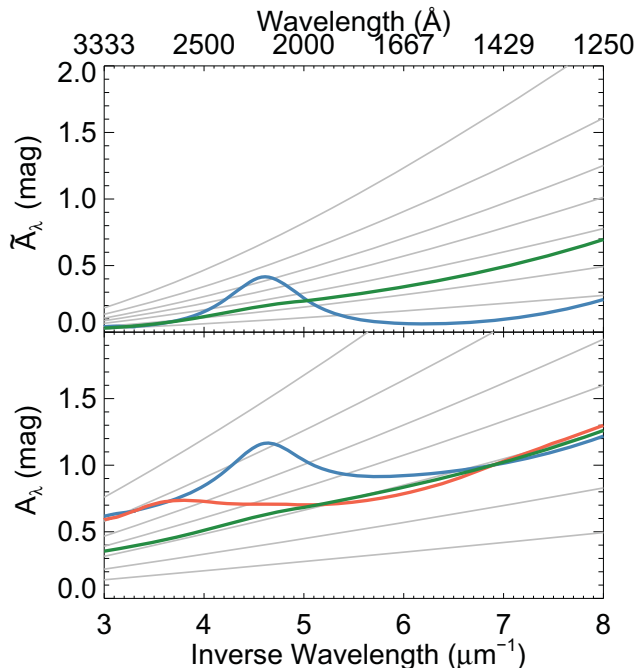
Figure 1. Absolute (bottom) and relative (top) extinction curves. Extinction curves are colored and normalized to $A_{1450} = 1$ mag (this corresponds to $A_V = 0.195$ mag for the SMC curve): Milky Way (blue), SMC (green), Todini–Ferrara theoretical extinction curve for SN dust (red). The Todini–Ferrara extinction curve is only plotted in the bottom panel because it is not defined above 3200 Å. Artificial extinction curves are shown in gray and are not normalized. They are obtained from a thermal disk assumed to be a power law for $T^* = 40, 50, 60, 70, 85, 120, 190 \times 10^3$ K (from top to bottom), as discussed in Section 2.1. Note the strong similarity to the SMC curve.

very blue QSOs are more likely to have a significant contribution from a thermal accretion disk (Pereyra et al. 2006) which is different from the usually assumed intrinsic power-law spectrum. Hence, it would be important to test if intrinsic slopes are indeed very blue and, if so, to probe fainter QSOs which would allow extinction measurements in systems with normal intrinsic spectral slopes.

There is only one example so far of a QSO, SDSS J1048+4637, with an observed extinction curve exhibiting a characteristic bump at around 3000 Å (Maiolino et al. 2004) similar to the theoretical extinction curve of Todini & Ferrara (2001). Stratta et al. (2007) did claim evidence for SN dust in GRB 050904, but this was later refuted by Zafar et al. (2010), as acknowledged by Stratta et al. (2011). Perley et al. (2010) and Jang et al. (2011) have reported a Todini & Ferrara (2001) like extinction curve in GRB 071025, which however relies on a photometric redshift and hinges on the precision of the calibration of the H-band measurements. G10 did interpret the somewhat shallower UV slopes found in their extinction curves as being consistent with SN dust, however, of a kind with no features in the extinction curves (Hirashita et al. 2008). It remains to be proven that an extinction curve with a UV slope, which is slightly shallower than the average SMC curve, would necessarily require SN dust, considering that radiative transfer effects will also give rise to shallower slopes and in view of the diversity of UV extinction curves in the Milky Way and the SMC (Cardelli et al. 1989;

Fitzpatrick & Massa 2007; Gordon et al. 2003). Thus, observationally, unusual extinction curves are in need of confirmation.

Regarding theoretically predicted extinction curves of SNe, there are considerable differences (Todini & Ferrara 2001; Bianchi & Schneider 2007; Hirashita et al. 2008, G10). The underlying dust formation models are sensitive to assumptions about the parameters controlling the dust grain properties (such as morphology, size or composition, Gall et al. 2011c; Fallest et al. 2011) which determine the shape and characteristics of extinction curves (see Section 6.5). Furthermore, dust grains produced by SNe will be subject to either disruptive, destructive or growth processes due to, for example, shock interactions in the SN remnant (e.g., Bianchi & Schneider 2007; Nozawa et al. 2007; Dunne et al. 2009; Matsuura et al. 2011) or the interstellar medium (e.g., Draine 2009; Michałowski et al. 2010a), or due to reprocessing by the intense UV radiation in star-forming regions. Any modifications of the original dust grains formed by SNe will lead to changes in either the mineralogy or the grain-size distribution of the dust, and hence the resulting extinction law (e.g., Hirashita & Kuo 2011). It is therefore not obvious to what extent the theoretical predictions of dust extinction curves from SN models are directly relevant to extinction curves inferred from lines of sight to QSOs. Therefore, it would be prudent not to rely on specific parametrizations when inferring extinction curves in high-redshift QSOs. A non-parametric approach is desirable because we cannot assume that current model predictions are correct or directly applicable to observational data.

Thus motivated, this paper is devoted to a study of possible extinction signals in high-redshift QSOs observed by the Infrared Array Camera (IRAC) on the *Spitzer Space Telescope.* We first discuss the procedures of inferring QSO extinction, including the choice of intrinsic spectrum, specifically power-law models vs. accretion disk models (Section 2). Next we show that the long-wavelength IRAC/*Spitzer* data allow us to constrain the intrinsic spectral slopes of the QSOs and use these to determine rough broad-band extinction curves for the full sample of QSOs (Section 3). In Section 4 we present X-shooter observations of high-redshift QSOs, which, combined with IRAC/*Spitzer* data, allow us to detect extinction in high-redshift QSOs with normal colors and little extinction. The targets are the broad absorption line (BAL) QSO SDSS J1044−0125 at $z = 5.78$ with a large inferred dust mass and the (non-BAL) QSO SDSS J1030+0524 at $z = 6.31$ with no sub-mm detection. Dust extinction has not been detected in these systems previously (G10). Finally, we study the prototypical system for a special SN extinction curve, SDSS J1048+4637, and show that there is no strong evidence for the previously claimed kink in the extinction curve (Section 5). We discuss our results in Section 6.

2. INFERRING DUST EXTINCTION CURVES IN QSOS

In this section we address the problem of inferring dust extinction in QSOs from the wavelength-dependent attenuation of the emitted light. The standard method of obtaining an extinction curve is to measure the ratio between an extinguished spectrum and that of a refer-

ence spectrum, typically an unextinguished object or a model spectrum. For example, multiply imaged (gravitationally lensed) QSOs have been used successfully to measure extinction curves of intervening (lensing) galaxies (Jaunsen & Hjorth 1997; Falco et al. 1999; Toft et al. 2000; Motta et al. 2002; Elíasdóttir et al. 2006) and power-law forms to measure extinction curves using gamma-ray burst afterglows (e.g., Zafar et al. 2010).

However, to measure extinction curves from the spectra of unlensed QSOs one must resort to comparing the observed spectrum with a model intrinsic spectrum. The interpretation of any signal may strongly hinge on the assumed shape of the intrinsic spectrum.

It is believed that a thermal accretion disk is responsible for the majority of the emission in the UV-optical regime of QSOs (Shang et al. 2005; Pereyra et al. 2006; Kishimoto et al. 2008; Lawrence 2012). On the other hand, it is standard practise to describe the continuum emission in QSOs as a power law, $f_\nu \propto \nu^\alpha$, i.e., $f_\lambda \propto \lambda^{-2-\alpha}$, presumably resulting from reprocessing of the flux from the thermal disk.

A thermal disk model is defined as

$$f_\lambda = \left(\frac{6G}{c^2}\right)^2 M_{BH}^2 \int_1^\infty \frac{8\pi^2 hc^2/\lambda^5}{\exp(hc/(\lambda k T^* t(s))) - 1} 4\pi s\, ds \tag{1}$$

with $t(s) = [s^{-3}(1 - s^{-1/2})]^{1/4}$ and characteristic temperature

$$T^* = \left(\frac{\dot{M}_{acc} c^6}{576\pi G^2 M_{BH}^2 \sigma_S}\right)^{1/4} \tag{2}$$

(Shakura & Sunyaev 1973; Shields 1978; Frank et al. 1992; Pereyra et al. 2006). In the above expressions, G is the gravitational constant, c is the speed of light, M_{BH} is the black-hole mass, h is Planck's constant, k is Boltzmann's constant, $\dot{M}_{acc}$ is the mass accretion rate, σ_S is the Stefan–Boltzmann constant, and s is the radius divided by the innermost disk radius. The latter is taken to be the last stable orbit for a non-rotating black hole, i.e., 3 times the Schwarzschild radius. The characteristic temperature T^* uniquely controls the shape of the thermal disk spectrum. For $\lambda T^* \to \infty$ the spectrum asymptotically approaches an $\alpha = 1/3$ power law.

In Figure 2 we show a thermal disk model as well as a power-law model for the continuum of a template QSO spectrum. It is evident that a power-law model (with $\alpha = -0.46$) provides a better description of the underlying QSO spectrum (i.e., unaffected by emission lines) at wavelengths redward of Lyα. A thermal disk model with $T^* \approx 85000$ K provides a reasonable approximation, but overshoots the continuum of the template spectrum in the range 0.13–0.23 μm. To avoid overshooting requires $T^* \lesssim 60000$ K, but such models severely underrepresent the UV portion of the spectrum.

2.1. Artificial extinction curves from accretion disk spectra modeled as power laws

If the assumed intrinsic model spectrum is wrong, then the method of obtaining extinction laws relative to this model will lead to spurious signals. For example, if the intrinsic spectrum is not a power law but modeled as such, results mimicking standard extinction laws could be inferred, even in the absence of dust. To quantify
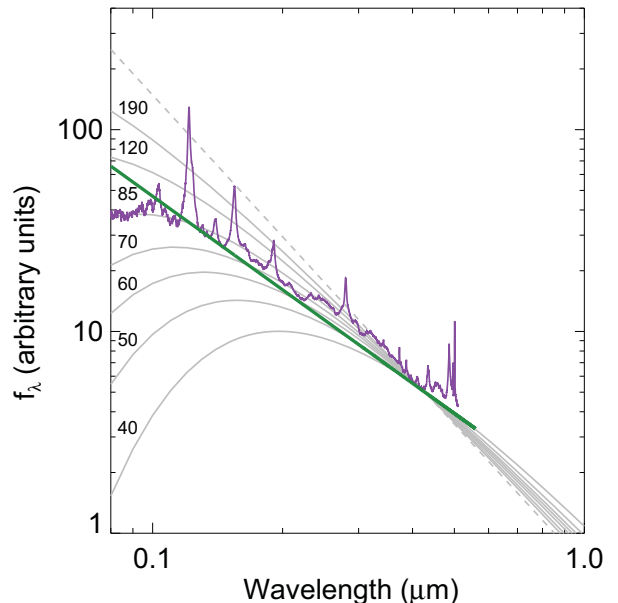

Figure 2. QSO template spectrum and models. Standard thermal disks with a range of characteristic temperatures are plotted as gray curves ($T^* = 40, 50, 60, 70, 85, 120, 190 \times 10^3$ K from bottom to top, solid curves and $T^* \to \infty$, dashed line). Also plotted is an *HST*/SDSS template spectrum (violet, based on Telfer et al. (2002) and Vanden Berk et al. (2001)). None of the thermal disk models provide acceptable representations of the template spectrum continuum. For example, the $T^* \approx 85000$ K model overshoots the continuum of the template spectrum in the range 0.13–0.23 μm. Between 0.13 μm and 0.50 μm a power law with spectral index $\alpha = -0.46$ (green line) is a better fit than the thermal disk, considering the effects of the broad emission lines (Vanden Berk et al. 2001). The SDSS template spectrum is not plotted above the location of [O III] λ5007 where it is likely contaminated by host galaxy emission. This is not expected to be an issue for the high-redshift QSOs studied in this paper.

the effect of a thermal contribution to the UV-optical spectrum of a QSO we compute the artificial extinction signal inferred when assuming a power-law intrinsic spectral distribution for a continuum described by a standard thermal accretion disk.

To obtain an effective extinction curve from a thermal model we (wrongly) assume the thermal accretion disk to be a power law between 5150 Å and 8300 Å (to mimic the analysis in the following sections) and compute the ratio between the accretion disk spectrum and the power law. The results are shown in Figure 1. We retrieve featureless 'extinction laws' which are similar to, but not identical to, the SMC extinction curve. The inferred 'extinction' is anti-correlated with the intrinsic temperature of the disk. This effect must be kept in mind when interpreting observational results although we recall that Figure 2 demonstrates that the contribution from such a thermal spectrum cannot be dominant.

For the analysis of observational data, we will therefore assume a power-law continuum model between Lyα and up to 8300 Å. This is not a good assumption at longer wavelengths where hot dust emission has been shown to dominate the emission in most high-redshift QSOs (Jiang et al. 2006, 2010). We discuss hot dust contamination in Section 3.2 and quantify the effect of a thermal disk contribution on our extinction measurements in Sec-
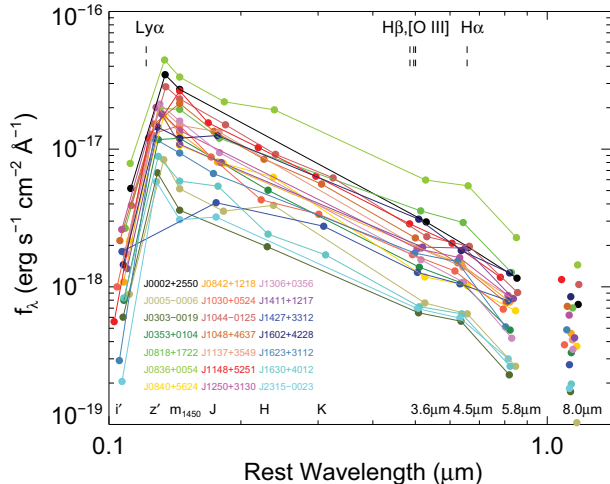
Figure 3. Optical/NIR and IRAC/*Spitzer* broad-band data for 21 $z \sim 6$ QSOs from Jiang et al. (2006, 2010). The data points are not plotted at fixed rest wavelengths because of the range in redshift ($5.78 \leq z \leq 6.42$). Note the conspicuous effects of the emission lines of Lyα and Hα in the z and 4.5 μm bands, respectively. For clarity, error bars are not plotted. The typical photometric uncertainties are 10–20 % in the optical/NIR bands and for the 5.8 and 8.0 μm IRAC bands and at the percent level for the 3.6 and 4.5 μm data points.

tion 3.3.

3. *Spitzer* SAMPLE OF $Z \sim 6$ QSOS

We used IRAC/*Spitzer* photometry of 21 $z \sim 6$ QSOs supplemented by tabulated (but non-simultaneous) optical and near-infrared broad-band photometry published by Jiang et al. (2006, 2010). The optical and near-infrared data were corrected for Galactic extinction (Schlegel et al. 1998) assuming $R_V = 3.1$. These corrections are small, with $E(B - V)$ ranging from 0.01 to 0.1 mag with the exception of SDSS J0353+0104 for which $E(B - V) = 0.29$ mag. The median value is $E(B - V) = 0.03$ mag. Such small Galactic extinctions are reassuring because the possible systematic biases on the QSO extinction signals from foreground extinction removal are thereby minimized.

In Figure 3 we show the resulting broad-band spectral energy distributions. We do not plot the 24 μm data points because they are dominated by hot dust emission in most cases. The 3.6 μm, 4.5 μm, and 5.8 μm data points do not seem to be affected (Jiang et al. 2006, 2010). The 8.0 μm data points are in some cases contaminated by hot dust emission. For this reason, these data points are not included in our analysis but shown in Figure 3 to illustrate the effect. Unfortunately, the 4.5 μm photometry is significantly affected by Hα emission at $z \sim 6$ and the 3.6 μm less so by Hβ and [O III] $\lambda\lambda4959, 5007$ emission (see Figure 2).

3.1. *Correction for emission-line contamination*

We correct the IRAC photometry for contamination by broad emission lines as follows. It is evident from Figure 3 that while there is a clear bump in the 4.5 μm band there is no conspicuous effect in the 3.6 μm band. For each QSO we therefore fit a power law to the 3.6 μm and 5.8 μm fluxes and estimate the excess
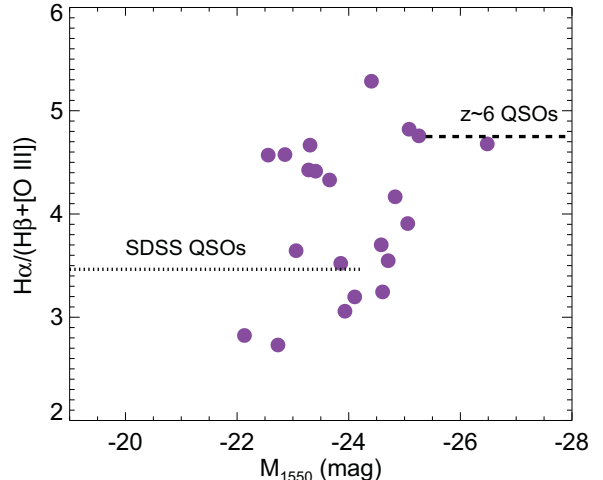

Figure 4. Relation between Hα to Hβ+[O III] equivalent width ratio and luminosity of the QSOs. The data points are for $z < 0.4$ Palomar–Green QSOs (Shang et al. 2007). The SDSS QSO template ratio (Vanden Berk et al. 2001) is indicated as a dashed line spanning the range of SDSS QSO absolute magnitudes. The dotted line indicates the ratio adopted in our analysis, spanning the range of absolute magnitudes of the $z \sim 6$ QSOs.

Hα flux. The median excess flux is 25%, corresponding to an Hα equivalent width of ~ 460 Å. This value is larger than for the template SDSS spectrum (194 Å; Vanden Berk et al. 2001) and consistent with the median value for the complete sample of $z < 0.4$ Palomar–Green QSOs (434 Å; Shang et al. 2007). This strongly suggests that the bump is indeed due to Hα emission and supports our method of analysis. We then correct the 3.6 μm band using an assumed equivalent width emission-line contamination ratio, $\eta \equiv$ H$\alpha/($H$\beta+$[O III]$)$. The template SDSS spectrum (Vanden Berk et al. 2001) suggests $\eta = 3.5$ while the brighter Palomar–Green QSOs yield a median $\eta = 4.2$, ranging from 2.7 to 5.3 (Shang et al. 2007), with a trend for more luminous QSOs to exhibit larger η (Figure 4). These QSOs are on average an order of magnitude brighter than the $z < 0.4$ SDSS QSOs making up the region around Hα and are therefore likely more relevant for our purposes. According to Figure 4, a ratio of $\eta = 4.75$ appears to be a reasonable value for luminous QSOs, which we adopt in what follows. We note however that an even higher ratio could in principle be relevant for some of the highly luminous $z \sim 6$ QSOs.

Taking into account the relative wavelength ranges of the relevant IRAC filters gives a ratio of 3.5 between the Hα to Hβ+[O III] emission-line to continuum contamination, which we apply to the 3.6 μm flux. The procedure was repeated by refitting a power law to the corrected 3.6 μm and 5.8 μm fluxes until convergence and resulted in a median correction of -8% to the 3.6 μm flux. The uncertainty in the correction induces a small systematic uncertainty in the inferred intrinsic power-law slope, α, which we address below.

3.2. *Extinction*

The relative extinction curve, $\tilde{A}(\lambda)$, for each QSO is obtained as the ratio between the restframe UV photometric data points and the extrapolated power-law model restframe optical spectrum, corrected for emission lines
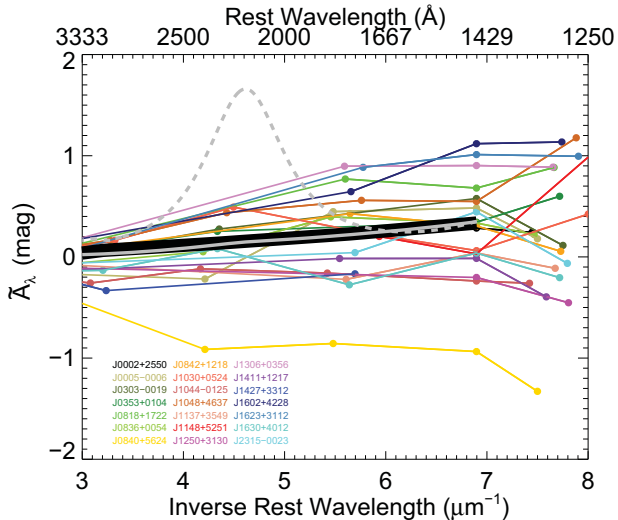
Figure 5. Broad-band extinction curves relative to the IRAC/*Spitzer* power-law baseline for 21 $z \sim 6$ QSOs. The thick black curve, with an indicative error of $0.20/\sqrt{21} = 0.04$ mag, is the median extinction curve of the 21 QSOs while the gray curve is a representative SMC extinction curve with $\tilde{A}_{1450} = 0.33$ mag. Note that for the SMC, $A_V \approx 0.41 \tilde{A}_{1450}$. A 2175 Å bump, characteristic of the Milky Way extinction curve (dashed gray curve), is not seen in the median extinction curve. There is no conspicuous 3000 Å kink either.
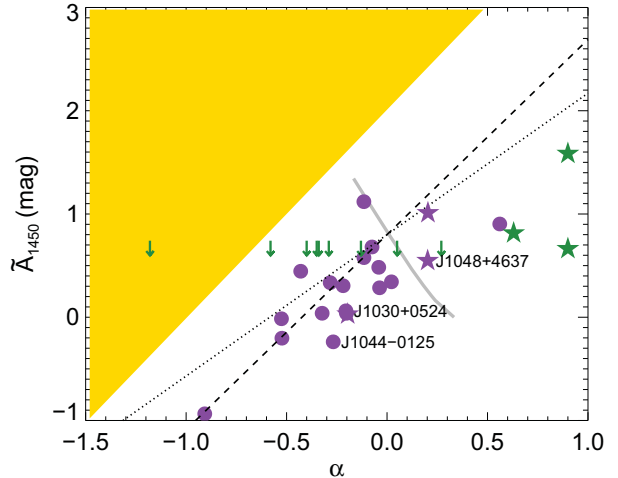

Figure 6. Spectral slopes versus extinction ($\tilde{A}_{1450}$, violet symbols) for 21 IRAC/*Spitzer* $z \sim 6$ QSOs. Also shown are the results of G10 (green symbols, stars for detections, arrows for upper limits). We used the G10 appropriate mean extinction curve or the extinction curves of individual objects to obtain A_{1450} from their A_{3000} and assumed the SMC extinction law relation $\tilde{A}_{1450} = 0.47 \tilde{A}_{1450}$ to obtain $\tilde{A}_{1450}$. Our corresponding results for the three green stars are shown as violet stars. The dashed and dotted lines indicate the degeneracies between $\tilde{A}_{1450}$ and α discussed in the text. The yellow region represents an exclusion zone due to the selection effect that reddened QSOs with a given IRAC 5.8 μm flux are more easily detected when the QSO is blue. The borderline between the excluded (yellow) and allowed region represents a QSO with an intrinsic $\alpha = 0$ spectrum, detectable at 10 σ at 5.8 μm and observable to $z' = 20.9$ mag in the SDSS. The gray line indicates the relation between excess inferred reddening and inferred spectral slope for a pure thermal disk, ranging from values around $\alpha \approx -0.2$, $\tilde{A}_{1450} \approx 1.3$ for low temperatures ($T^* \approx 40000$ K) to the asymptotic values ($\alpha = 0.33$, $\tilde{A}_{1450} = 0$) at high temperatures.

as explained above. Figure 5 shows the resulting extinction curves. There is significant scatter in the data, which are affected by other emission lines, depending to some extent on the actual redshift of each QSO. Variability may also play a role in some cases. Finally, there are substantial photometric uncertainties associated with the optical and near-infrared photometry corresponding to about 0.1–0.2 mag (Jiang et al. 2010).

Nevertheless, it is evident that the curves do not scatter around zero. If the data were dominated by intrinsic variability, they would scatter symmetrically around the zero mean. This is not the case. There is a clear positive effect, as expected if the QSOs are reddened relative to a power-law spectrum. The effect is relatively small, however, with values reaching a maximum of about 1 mag in the restframe UV. Only one out of 21 QSOs (SDSS J0840+5624 at $z = 5.85$) appears to exhibit a significant negative signal. This may be due to variability between the epochs at which the SDSS photometry, the near-infrared photometry, and the IRAC/*Spitzer* photometry were obtained. Alternatively, since we are relying on deriving a slope from just two literature data points, we cannot exclude problems with the reported photometry. In fact, the 8.0 μm data point for this target seems to indicate a somewhat steeper spectral slope which would give rise to a less negative or even positive extinction signal.

The data are not of sufficient quality to obtain the detailed shapes of the individual extinction curves. The median extinction curve is consistent with an SMC curve with $A_V = 0.13$ mag while a Milky Way 2175 Å bump is strongly ruled out. Likewise, there is no conspicuous 3000 Å kink.

For each QSO we can obtain an estimate of the UV extinction, $\tilde{A}_{1450}$, from the 1450 Å magnitude (the z and J bands are affected by Lyα and C IV emission, respec-

tively). Figure 6 shows the relation between the inferred extinction, $\tilde{A}_{1450}$, and spectral slope, α. There is a clear correlation, which can be understood as follows: For a power, law $f_\nu \propto \nu^\alpha$, anchored at $\lambda_{\rm anchor}$ and observed at $\lambda_{\rm obs}$ the difference in the inferred relative extinction at $\lambda_{\rm obs}$ is

$$\delta \tilde{A} = 2.5 \log \left(\frac{\lambda_{\rm anchor}}{\lambda_{\rm obs}} \right) \delta \alpha \qquad (3)$$

if the spectral slope changes by $\delta \alpha$.

One uncertainty in α arises from the slightly model dependent correction for the flux of Hβ and [O III] in the 3.6 μm band. The spectral slope is anchored at the 5.8 μm IRAC band, i.e., at around 8300 Å in the restframe at $z = 6$. The observed wavelength is at 1450 Å in the restframe. Hence, we expect the inferred extinction and spectral slope data points to be degenerate along

$$\delta \tilde{A} = 1.89 \delta \alpha, \qquad (4)$$

plotted as a dashed line in Figure 6. We find that a variation $\delta \eta$ leads to a change in α of

$$\delta \alpha \approx 0.1 \frac{\delta \eta}{4.75}, \qquad (5)$$

which indicates that this is a small effect.

Another source of error is the possible contamination of the 5.8 μm band by hot dust emission. If this uncertainty is dominant, the spectral slope is effectively anchored at the 3.6 μm IRAC band, i.e., at around 5150 Å in the

restframe at $z = 6$, and

$$\delta \tilde{A} = 1.37 \delta \alpha. \tag{6}$$

This relation is plotted in Figure 6 as a dotted line. We find that the median value of α in this case varies as

$$\delta \alpha \approx -1.8 \frac{\delta f_{5.8\mu m}}{f_{5.8\mu m}}, \tag{7}$$

which shows a strong sensitivity to the 5.8 μm flux. Fortunately, the hot dust contamination at 8.0 μm is small ($\lesssim 10\%$, see Figure 3) and hence negligible in most cases at 5.8 μm: the Planck function drops by a factor of 9 between 8.0 μm and 5.8 μm in the Wien region, while the flux is roughly constant for $\alpha \approx 0$. This is consistent with the hot dust models of Jiang et al. (2006) which indicate that the contamination of the 5.8 μm flux is of order 1%. We note that any contamination by hot dust emission will cause the 5.8 μm flux to be overestimated and hence α and $\tilde{A}$ to be underestimated. For consistency, we applied a -1% correction to all 5.8 μm fluxes to account for contamination by hot dust emission.

Having shown that the systematic uncertainties related to the choice of η or due to hot dust contamination are small, we conclude that the actual photometric uncertainty in the 5.8 μm flux dominates the error budget (the uncertainties in the 3.6 and 4.5 μm fluxes are much smaller). The median relative error in the 5.8 μm flux is 8% which translates into a typical error in $\tilde{A}_{1450}$ of 0.20 mag, or 0.04 mag in the mean for the sample of 21 QSOs.

Selection effects are described by relations similar to Equations (4) and (6). As the selection of high-redshift QSOs is based on a z'-filter detection and i'-filter dropout, the dominating selection effect is related to the z'-filter brightness. For a given IRAC 5.8 μm band detection, the corresponding constant of proportionality in Equation (4) becomes slightly larger, around 2 (taking the z'-band to be the observed wavelength), i.e., it defines an exclusion zone above a line with a slope of $\delta \tilde{A}_{1450}/\delta \alpha = 2$ where QSOs are too faint for detection. The normalization depends on the intrinsic brightness of the QSOs and the depth of the IRAC/*Spitzer* observation. In Figure 6 we illustrate the effect for a typical QSO detected at 100 ± 10 μJy in the 5.8 μm band. Assuming a flat spectrum ($\alpha = 0$) this corresponds to a QSO with an unextinguished brightness of $z' = 18.9$ mag. The faintest QSO in the sample has $z' = 20.9$ mag, i.e., we can observe 2 mag of relative extinction for a QSO with $\alpha = 0$. G10 discussed a color selection effect based on $z' - J$ but this constraint is weaker than the brightness constraint in our case and is not plotted.

3.3. *Discussion of the broad-band results*

Figure 6 illustrates the fact that available detection limits do not allow the detection of very reddened QSOs with small spectral slopes (i.e., intrinsically red QSOs). Therefore, as pointed out by G10, the fact that previously reported high-redshift QSOs with significant extinction are intrinsically very blue appears consistent with the selection effects. On the other hand, our results appear to be inconsistent with the G10 results. In Figure 7 we compare the spectral slopes obtained for the QSOs studied here with those obtained by G10. There is no obvious correlation between the respective values and no systematic bias either. It seems the outcomes
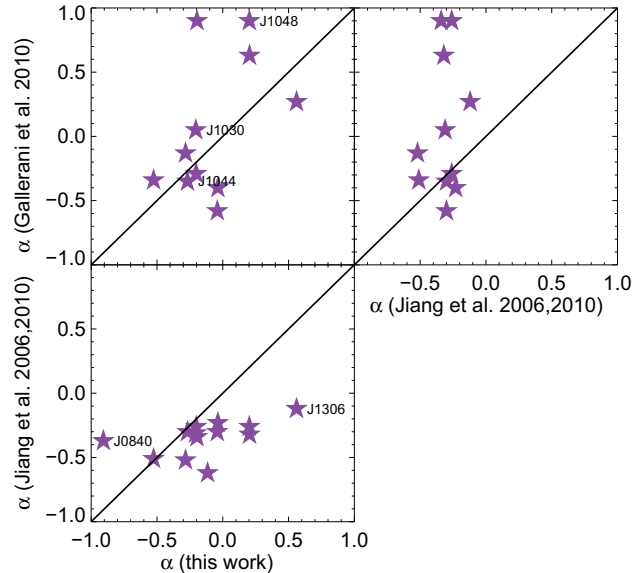

Figure 7. Comparison of inferred spectral slopes for $z \sim 6$ QSOs. We plot the intrinsic spectral slopes obtained in this work and compare to those of G10 and those adopted by Jiang et al. (2006, 2010). The filled stars represent QSOs for which α is reported by the different sources. The symbols should lie on the solid lines for consistency between the different methods for inferring the intrinsic spectral slopes. Note that our slopes and those of G10 are extinction corrected whereas those of Jiang et al. (2006, 2010) are not. This partly explains why the latter values are smaller, corresponding to redder sources.

of the two approaches are very different. Hence, given the extinction–spectral slope correlation, extinctions obtained in at least one of the approaches may be unreliable. In the sample of 3814 SDSS QSOs studied by Reichard et al. (2003), QSOs with observed slopes of $\alpha \approx 1$ or bluer are extremely rare. Davis et al. (2007) find an even more restricted range of slopes in the 1450–2200 (2200–4000) Å range from 3646 (2706) quasars with redshifts in the $z = 1.67$–2.07 (0.76–1.26) range. QSOs with $\alpha > 0.5$ are practically non-existent in this sample. Hence, for G10 to find three extremely blue ($\alpha > 0.6$) $z \sim 6$ QSOs seems unlikely. None of our values of α are this extreme. Our median value of $\alpha \approx -0.2$ may be compared to the SDSS template slope of -0.46 and the mean slopes of -0.59 (1450–2200 Å) and -0.37 (2200–4000 Å) found by Davis et al. (2007). This may indicate a slight bias towards blue QSOs, which may partly be due to a selection effect because even little extinction would make intrinsically red QSOs undetectable.

As discussed above, the main weakness of the approach adopted by G10 is that it relies on an assumed extinction curve, fitted over a limited range in wavelength, to regions of the spectrum which may not quite reach the true continuum level. Some of these weaknesses are eliminated in our approach, however, at the expense of not determining absolute extinction values: We emphasize that the extinction curves obtained here are relative to the 3.6–5.8 μm power law model and in this sense are not absolute but strictly lower limits (for an SMC extension above 3000 Å, $\tilde{A}_{1450} \approx 0.5 A_{1450}$, see Figure 6).

As such, our approach is insensitive to a possible gray (i.e., wavelength independent) extinction compo-

nent. However, for an entirely gray extinction curve our approach would have led to zero relative extinction to be detected. The fact that there is a clear positive detection implies that the typical extinction curve of high-redshift QSOs is wavelength dependent, giving rise to reddening as expected (still under the assumption of an intrinsic power-law spectrum).

To address the question of systematic errors in the derived extinction values due to a contribution of a thermal disk we overplot the extinction–slope relation inferred for a non-reddened thermal accretion disk model in Figure 6. The curve reflects a range of characteristic temperatures starting at $T^* = 40000$ K ($\alpha = -0.2$, $\tilde{A}_{1450} = 1.3$ mag) and approaching the asymptotic value ($\alpha = 0.33$, $\tilde{A}_{1450} = 0$) for large T^*. Remarkably, this curve is practically perpendicular to the degeneracy relations, Equations (4) and (6), so basically adds to the scatter in this relation. Moreover, it is evident that the results do not span the full range of temperatures plotted, preferring values in the range $T^* = 60000$–100000 K. Interestingly, the fact that the majority of the points do not lie on this relation shows that the QSO spectra are not well described by pure thermal disks and require a significant additional component, such as the power law assumed in our analysis.

4. X-SHOOTER OBSERVATIONS

4.1. *Targets*

4.1.1. *SDSS J1030+0524*

SDSS J1030+0524 (Fan et al. 2001) is a $z = 6.309 \pm 0.009$ QSO (Jiang et al. 2007; Iwamuro et al. 2004). Priddey et al. (2003) obtained an upper limit to the dust mass of 1.4×10^8 M$_\odot$ from SCUBA observations. The source is located in a crowded sub-mm field. The sub-mm sources in the field are, however, likely due to foreground galaxies (Priddey et al. 2008). A deep X-ray spectrum did not reveal evidence for X-ray absorption ($N_H < 8 \times 10^{22}$ cm^{-2}; Farrah et al. 2004). Jiang et al. (2006) find a hot dust mass larger than 17 M$_\odot$. There are Lyα emitters in the field at $z = 5.7$, one consistent with being a foreground absorber (Gonzalo Diaz et al. 2011) in the QSO spectrum. There is also a strong Mg II absorber at $z = 2.780$ (Simcoe et al. 2011). Jiang et al. (2010) report a black hole mass of 2.75×10^9 M$_\odot$.

4.1.2. *SDSS J1044−0125*

SDSS J1044−0125 (Fan et al. 2000) is a BAL QSO (Maiolino et al. 2001; Djorgovski et al. 2001; Goodrich et al. 2001; Freudling et al. 2003) at $z = 5.778 \pm 0.004$ (Jiang et al. 2007) with a large cold dust mass of 4.2×10^8 M$_\odot$ (Priddey et al. 2003) and a hot dust mass larger than 53 M$_\odot$ (Jiang et al. 2006) (second highest in the sample). It could be magnified by at most a factor of 2 due to gravitational lensing (Shioya et al. 2002; Wyithe 2004) so the derived properties are likely not strongly overestimated. Jiang et al. (2010) find a black hole mass of 10.5×10^9 M$_\odot$.

4.2. *Observations*

We observed SDSS J1044−0125 and SDSS J1030+0524 on 22 and 23 December 2009 UT, respectively, with the X-shooter spectrograph (D'Odorico et al. 2006;

Vernet et al. 2011) mounted at the Cassegrain focus of the *Kueyen* unit of the Very Large Telescope (VLT) at the European Southern Observatory (ESO), Cerro Paranal, Chile. The observations started at around 7 UT on both nights, and consisted of a set of 4×1200 s integrations, with the objects being offset along the slit between the exposures. The seeing as measured from the guide stars used for the QSO observations was approximately $0.7''$ for both nights. During the SDSS J1044−0125 observations thin clouds were scattered across the sky, while the sky was clear during the next night when SDSS J1030+0524 was observed. The approximate airmass range for both QSO observations was 1.1–1.3, i.e., with a maximum zenith angle of 40 degrees.

X-shooter allows for simultaneous spectroscopic observations at intermediate resolution in three different arms: the ultra-violet and blue (UVB), visual (VIS) and near-infrared (NIR) wavebands, with a continuous spectral coverage of 0.3–2.5 μm. In this paper we only report results for the VIS and NIR arms as the UVB arm covers restframe wavelengths much smaller than Lyα (1216 Å). We used slit widths of $0.9''$ for both the VIS and NIR arms, resulting in resolving powers of 8800 (VIS) and 5600 (NIR). Immediately following the QSO integrations, a telluric standard star was observed at a very similar airmass and with the same instrument set-up as the QSOs, i.e., with the same slit widths and binning (no binning in the spatial direction, and two pixels in the dispersion direction for the VIS arm). During both nights, observations of spectrophotometric standards were also secured. The QSOs and the standards were all observed with the slit aligned with the parallactic angle.

Using version 1.2.2 of the X-shooter pipeline (see D'Odorico et al. 2006) in polynomial mode, the object, telluric and standard star spectra were reduced to two-dimensional bias-subtracted, flat-field corrected, order rectified and wavelength calibrated spectra in counts. One-dimensional spectra were optimally extracted from these (see Horne 1986) with a custom IDL routine.

We used the general version of the IDL-based *xtellcor* program developed by Vacca et al. (2003) for SpeX – a 0.8–5.5 μm medium-resolution cross-dispersed spectrograph at the NASA Infrared Telescope Facility – to perform a telluric correction and flux calibration of the QSO spectra. *Xtellcor* uses a high-resolution model spectrum of Vega that is scaled, reddened and convolved with the instrumental resolution to match the observed spectrum of a telluric standard as close as possible, including the hydrogen absorption lines. Comparison between the model and observed telluric spectra then allows for correction of the telluric features in the object spectra, and also provides a flux calibration if the B and V magnitudes of the telluric standards are known. The telluric spectra that we used were both observed immediately following the QSO: HIP 49704 for SDSS J1044−0125 and HIP 055011 for SDSS J1030+0524, at airmasses of 1.17 and 1.11, respectively; this is within 0.1 airmass of that of the QSO spectra. Both telluric standards are classified as stellar type B9, and are therefore very similar in type to an A0V star that is optimally suited for this telluric correction method. The advantage of using the telluric spectrum to also perform the flux calibration – using the Vega model – is that the telluric standard was taken immediately following the QSO, at a similar air-

mass, and with the same slit width, which minimizes slit loss differences.

We checked the flux calibration by applying the sensitivity function (which converts measured counts to absolute flux) inferred by the *xtellcor* program directly to a spectro-photometric standard star observed during the same night, and by comparing the resulting spectrum to tabulated flux values. For the SDSS J1044−0125 night we used observations of BD+17 4708 at airmass 2.63, while for the SDSS J1030+0524 night we used GD71 at airmass 1.45. These standards were observed with a 5″ wide slit. On both nights, we find that the inferred flux for these standards is a factor of 1.3 higher than the tabulated values, while this factor is constant across the spectra to within 5% – the approximate accuracy of the relative flux calibration. The offset of 30% could partly be attributed to slit losses (the telluric standards and QSOs were taken with a 0.9″ slit).

Given these absolute flux calibration offsets, we compared the resulting flux-calibrated spectra for the QSOs with the JHK magnitudes collected in Table 1 of Jiang et al. (2006). For SDSS J1044−0125 the spectrum flux values are consistent with the magnitudes within their errors (0.05–0.1 mag). However, for SDSS J1030+0524 the spectrum flux is too high by 30% as measured from the H and K bands where the f_λ is flat and void of spectral features.

This difference prompted us to check if the flux of either QSO is variable in time. We measured the magnitude of SDSS J1030+0524 from X-shooter z'-band acquisition images using aperture photometry and calibrated against the SDSS. We find $z' = 19.81 \pm 0.06$ on the night of 23 December 2009, while we find $z' = 19.93 \pm 0.04$ for the night of 8 February 2011 (taken from the ESO archive), i.e., reasonably consistent with being constant. This compares to $z' = 20.05 \pm 0.10$ as reported in the discovery paper of Fan et al. (2001). For SDSS J1044−0125, we measure a magnitude of $z' = 19.27 \pm 0.07$ from our acquisition images, while Fan et al. (2000) report $z' = 19.23 \pm 0.07$. No other X-shooter acquisition images, or a suitable series of images taken with other ESO instruments are available to check for flux variability of SDSS J1044−0125. The broad-band photometry is consistent with a marginally significant brightening of SDSS J1030+0524 of 0.24 ± 0.12 mag between 2000 and 2009, while SDSS J1044−0125 is consistent with being constant. These findings reflect the inconclusive spectroscopic results. Given that we do not have information of the brightness of SDSS J1030+0524 at the time of the IRAC/*Spitzer* observations we proceed by not making any corrections due to variability but note that a 30% brightness correction would offset the resulting extinction curve higher by about 0.30 mag.

Finally, we corrected the flux-calibrated QSO spectra for the Galactic extinction along the sightlines, with $E(B - V)$ of 0.024 for SDSS J1030+0524 and 0.051 for SDSS J1044−0125 using Schlegel et al. (1998). We display the X-shooter/VLT spectra in Figure 8.

4.3. *Extinction curves*

QSO spectra are strongly affected by emission lines, both bright conspicuous broad emission lines and fainter, blended lines giving rise to a quasi-continuum, especially around 0.2–0.3 μm, the so-called small blue bump due
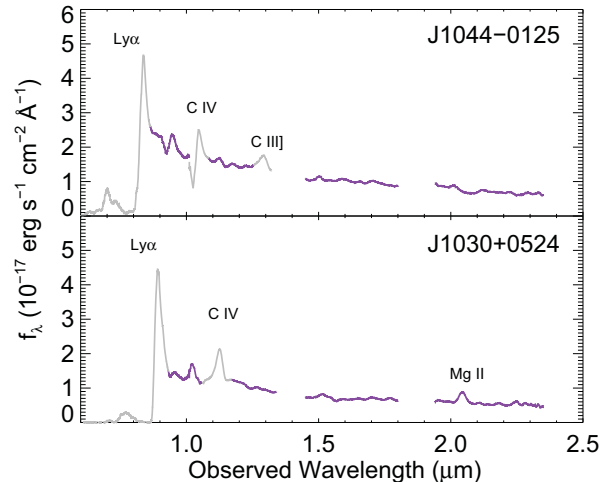

Figure 8. X-shooter/VLT spectra of SDSS J1030+0524 and SDSS J1044−0125. The gaps in the spectra are due to the main atmospheric absorption bands between the J and H band and the H and K band. Regions plotted in gray are not included in the analysis due to the presence of strong emission lines (see Figure 9), broad absorption, or intergalactic absorption. The main emission lines are indicated. The spectra have been smoothed to 0.02 μm resolution.
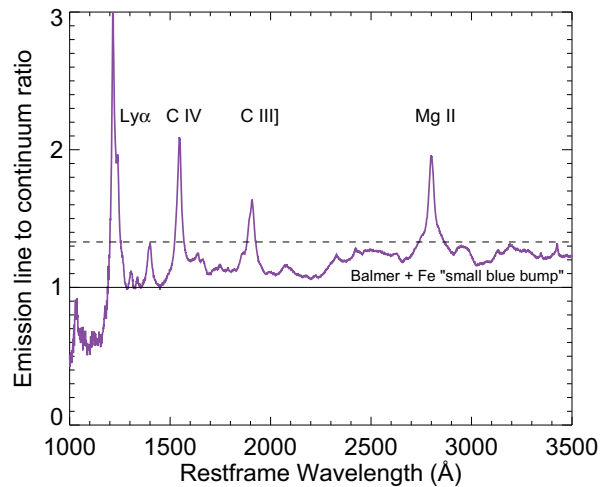

Figure 9. QSO emission-line to continuum ratio obtained as the ratio between the QSO template and the continuum model shown in Figure 2. The solid line represents identity between the QSO template and the continuum. Note that the continuum is not reached at any point above 1450 Å. The dashed line indicates regions above which the spectrum is severely affected by strong broad emission lines.

to Balmer and Fe II lines. It is essential to remove the contamination by these lines to determine the true continuum level, assumed to be a power law in our analysis. We use the Vanden Berk et al. (2001) SDSS QSO template to estimate the ratio between the QSO signal, affected by emission lines, and the continuum level (Figure 9). We divided the X-shooter spectra by this ratio to obtain an estimate of the quasi continuum, shown in Figure 10. It is evident that our procedure of removing the emission line contribution works reasonably well in these systems.
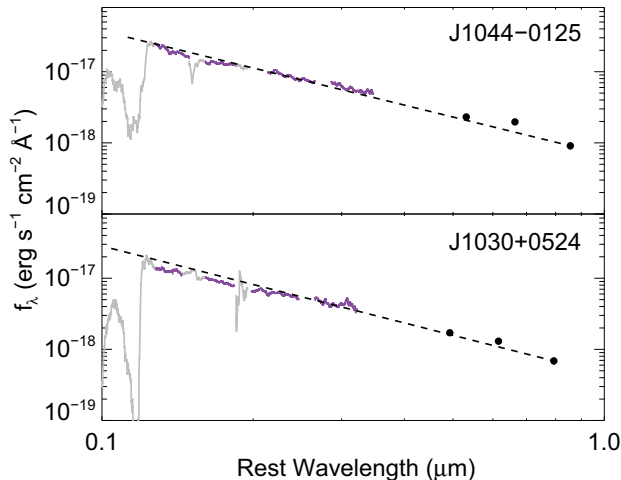
Figure 10. X-shooter/VLT spectra of SDSS J1030+0524 and SDSS J1044−0125 after correction for emission lines, see Figure 9. The filled circles are the IRAC/*Spitzer* data points. The dashed line is the adopted intrinsic power-law spectrum fitted to the IRAC data points as described in the text. The extinction is inferred as the ratio between the dashed line and the spectrum. As shown in Figure 11, the slight mismatch between the extrapolated power laws and the observed spectra are eliminated when choosing the 1σ lower boundary for the 5.8 μm fluxes.

Figure 11. Inferred X-shooter/VLT extinction curves for SDSS J1030+0524 and SDSS J1044−0125. The thick black line is a smooth 3rd order polynomial fit to the data. The thick dashed lines correspond to assuming the lower 1σ error on the 5.8 μm flux. If a 30% brightness correction is applied to the SDSS J1030+0524 spectrum (see Section 4.2) the resulting extinction curve would be offset higher by about 0.30 mag. Indicative relative SMC (solid) and MW (dashed) extinction curves are overplotted in gray.

We repeated the procedure of the previous section to tie the spectra of SDSS J1030+0524 and SDSS J1044−0125 to the IRAC/*Spitzer* data. We assume that there has been no variability of the QSOs and that the intrinsic continuum spectrum is well represented by a power law as fixed by the 3.6 μm and 5.8 μm IRAC data points, suitably corrected for emission lines. We can then determine the extinction law as the ratio between the extrapolated power law and the emission-line corrected X-shooter spectrum. The resulting extinction curves are presented in Figure 11.

The signals are not very strong, although there seems to be the expected reddening effect, with $\tilde{A}_{1450} = 0.14$ mag for SDSS J1044−0125 and $\tilde{A}_{1450} = 0.24$ mag for SDSS J1030+0524, consistent within the photometric errors with the broad-band values for these QSOs (Figures 5 and 6). Neither QSO had evidence for extinction in the G10 analysis, but their limits are fully consistent with our detections. The systematic errors in these extinction curves amount to $\pm \sim 0.25$ mag at 1450 Å for these systems because of the $\sim 11\%$ errors in their 5.8 μm fluxes. Nevertheless, we can rule out conspicuous features at 2175 Å (and to some extent 3000 Å). SDSS J1030+0524 has a UV rise which is slightly shallower than the SMC, while there is an apparent downturn in SDSS J1044−0125.

5. SDSS J1048+4637

An apparent UV-flattening was found in the extinction curve of SDSS J1048+4637, based on prism spectrophotometry using the Near Infrared Camera Spectrometer (NICS) instrument at the Telescopio Nazionale Galileo (TNG) and attributed to dust from SNe (Maiolino et al. 2004). In a reanalysis of the same data, G10 found that the presence of such a steep-flat-steep ('kinked') extinction curve was heavily dependent on the intrinsic slope
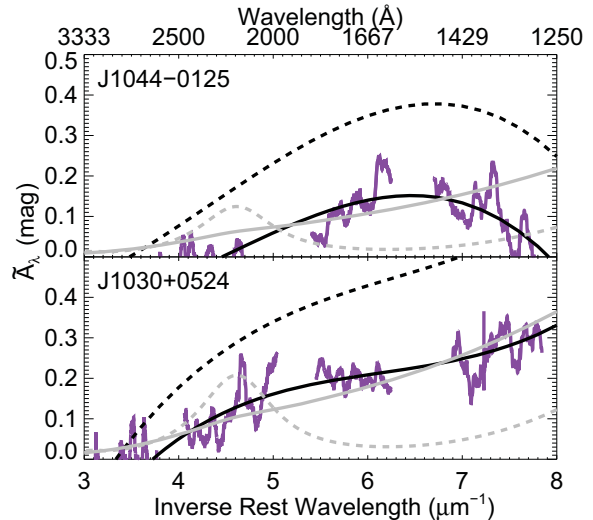
assumed. A different intrinsic slope resulted in a relatively flat extinction curve without a kink. We have attempted the construction of extinction curves for SDSS J1048+4637 using data from the literature, acquired using the SAO/NASA Astrophysics Data System's Dexter data extraction applet (Demleitner et al. 2001). Optical/NIR spectra were acquired from Maiolino et al. (2004), Iwamuro et al. (2004), Fan et al. (2003, 2006) based on data from NICS/TNG, from the OH-Airglow Suppressor/Cooled Infrared Spectrograph and Camera for OHS (OHS/CISCO) on Subaru, from the Low-Resolution Spectrograph (LRS) on the Hobby-Eberly Telescope (HET), and from the Echelle Spectrograph and Imager (ESI) on Keck.

These data were all analysed with the method described in Section 4.3. The resulting extinction curves using the TNG and the Subaru+Keck data, respectively, are shown in Figure 12 (we do not show the LRS/HET data which are consistent with the ESI/Keck data, but of lower quality).

The data from NICS/TNG result in an extinction curve similar to that found by Maiolino et al. (2004). There is however no conspicuous bump in the extinction curve, although a plateau is evident. In the combined ESI/Keck+OHS/CISCO/Subaru spectrum the overall normalization of the extinction curve is significantly lower and instead of a plateau there is a monotonically rising extinction towards the red. The shapes of the extinction curves do not seem very different though, with only a mild change of slope in the observed NIR. In both cases there is a UV upturn with a slope similar to the SMC.

The differences in the derived extinction curves may be due to variability and/or there may be instrumental causes. In case of variability the source would have had to vary by as much as 60% in the restframe UV to explain the difference in the absolute extinction level. In-
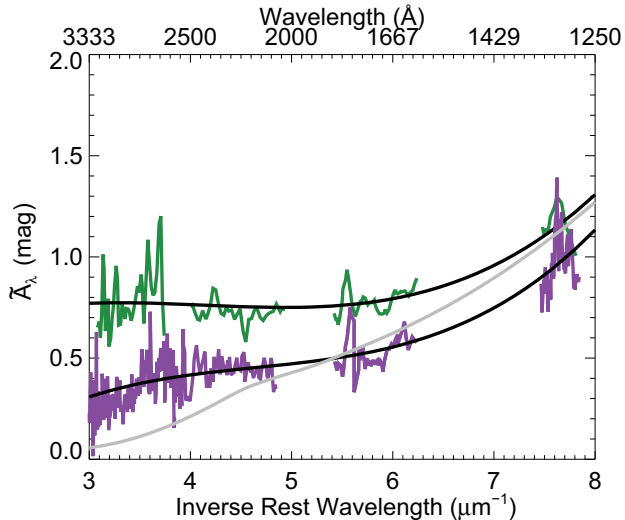
Figure 12. Relative extinction curves for SDSS J1048+4637. The green curve is based on our re-analysis of the NICS/TNG data (Maiolino et al. 2004) whereas the violet curve is based on a combination of ESI/Keck and OHS/CISCO/Subaru data. The black overplotted curves are 3rd order polynomial fits to the data, for illustration. For comparison with the ESI+OHS curve, the relative SMC extinction curve is overplotted in gray. The curves are consistent with a flattening longward of 1700 Å and a UV upturn shortward of 1700 Å, as discussed by Maiolino et al. (2004). There is no conspicuous kink in either curves but they are clearly inconsistent with an SMC-like relative extinction curve. Note that the relative G10 or Maiolino et al. (2004) curves cannot be plotted because they are not defined above 3200 Å.

strumental problems may play a role for the NICS instrument which is a very low resolution instrument, making sky-line subtraction complicated in the NIR. Conversely, NICS is a prism instrument and so is not susceptible to possible systematic slitloss correction errors in the way that the ESI and OHS/CISCO slit spectra may be.

We have to accept that the available data on SDSS J1048+4637 can only lead us to inconclusive results about its extinction curve. This could be resolved with well-calibrated, simultaneous optical-IR spectrophotometry in the future. Unfortunately, the object is unobservable with X-shooter/VLT due to its declination.

While we confirm that the flat extinction curve is inconsistent with a typical SMC curve, we cannot endorse the view that there is evidence for a kinked 'SN'-type extinction curve in this QSO, leaving no spectroscopic evidence for such a curve in any object to date. GRB 071025 is the only currently uncontested case of such an extinction curve (Perley et al. 2010). However, GRB 071025 has only a photometric redshift at $z \sim 5$ (which impacts on the wavelength scale of the extinction curve) and the detection of a kink relies on H-band photometry being accurate to a few percent.

6. DISCUSSION

6.1. *Inferring hot dust masses*

In the process of estimating extinction in high-redshift QSOs observed by IRAC/*Spitzer*, we have devised a careful method of estimating their intrinsic spectral slopes. The main systematic uncertainty in this method comes from estimating the parameter η which controls the correction for the emission lines entering the IRAC channels. Accurately estimating the intrinsic spectral slopes is also

important for inferring hot-dust masses of these QSOs. Poor estimates of the spectral slope could lead to biases in the inferred hot dust component as measured essentially in the IRAC 8.0 μm and 24 μm data. In Figure 7 we therefore compare our spectral slopes to those used by Jiang et al. (2006, 2010) in their estimates of the mass of hot dust in the targets. It is evident that their spectral slopes are generally lower than ours, which leads to an underestimate of the hot dust signal. In particular, the hot dust mass of SDSS J1306+0356 should probably be revised upwards because of its significantly higher spectral slope than that found by Jiang et al. (2006). Conversely, the hot dust mass of J0840+5624 may have to be revised downwards, although we note that this object was found to have spurious negative extinction, due to either variability or problematic photometric data (see Section 3.2).

6.2. *Correlations with other properties*

We compare our inferred spectral slopes and extinctions with other properties of the QSOs which might correlate with these values. In Figure 13 we plot the black hole masses, cold dust masses and hot dust masses for the sample, to the extent that the data are available. There are no obvious correlations between the inferred spectral slope or extinction with either the mass of the black hole or the mass of hot or cold dust. However, focusing in particular on the targets with sub-mm or mm detections or upper limits, Figure 13 shows that the systems with large amounts of cold dust (the filled symbols represent systems with sub-mm detections) also generally have large black hole masses and hot dust masses. Moreover, there is an indication that systems with significant extinction observed with SCUBA have sub-mm detections. This is encouraging and suggests that a significant part of the signal we find is indeed due to extinction and not an artifact of the data analysis or a thermal accretion disk.

6.3. *The case of SDSS J1044−0125*

Judging from Figure 13, SDSS J1044−0125 appears to constitute a somewhat peculiar case because it is a BAL QSO with large amounts of inferred cold and hot dust and a large black hole mass. Yet, we only find evidence for very little extinction. We note, however, that if we assume a typical dust-to-gas mass ratio, and a spherical dust distribution in the host galaxy of the QSO, with angular diameter $< 5''$ (Wang et al. 2010), we would anticipate $A_V \gtrsim 0.16$ mag for the QSO. We observe $\tilde{A}_{1450} \sim 0.14 \pm 0.24$ mag which corresponds to $A_V \approx 0.06 \pm 0.16$ for an SMC-like extinction curve (see Figure 1). These values are consistent within the uncertainties. Moreover, the dust distribution in SDSS J1044−0125 is likely not spherically distributed. For example, the galaxy may be flattened into a more disk-like shape. The relatively narrow width of the CO(6−5) line relative to the [C II] linewidth (Wang et al. 2013) indicates complex gas dynamics.

6.4. *Caveats*

We seem to consistently find positive signals for the extinction and there is some correlation with dust signals found using other methods. Nevertheless, as we have
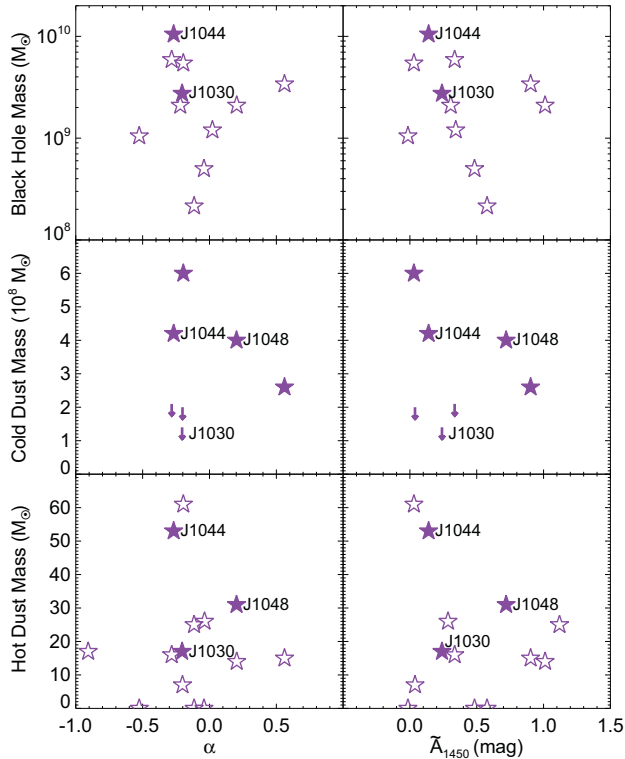
Figure 13. Black hole mass, cold dust mass and hot dust mass versus spectral slope and extinction (violet stars). Filled symbols represent QSOs with sub-mm detections, arrows in the middle row represent QSOs with sub-mm upper limits. The relative extinction values and spectral slopes for SDSS J1030+0524, SDSS J1044−0125, and SDSS J1048+4637 are based on the refined analysis of their spectra presented in this paper. The black hole masses and hot dust masses are from Jiang et al. (2006, 2010) and M. Vestergaard (private communication). The cold dust masses are from SCUBA 850 μm observations (Priddey et al. 2003; Robson et al. 2004; Priddey et al. 2008). Note that the two systems with $\tilde{A}_{1450} > 0.5$ mag which have been observed with SCUBA have detections of large masses of cold dust.

stressed throughout, our approach relies on a number of assumptions, which we summarize below, along with additional possible systematic errors.

- Likely, the most important caveat is the unknown shape of the intrinsic spectrum, as we have discussed at some length. The assumption of a power law is a convenient one, for lack of a better credible and operational model for the intrinsic spectrum of a QSO.

- We have estimated the effect of a thermal spectrum and shown that the effect is limited and perpendicular to the effect of extinction in the extinction–spectral slope plane (Figure 6). Moreover, we have attempted to take out the effect of emission lines by dividing out a template excess continuum spectrum based on SDSS QSOs (Figure 9). On the other hand, the fake accretion disk extinction curves are quite reminiscent of the inferred extinction curves and we cannot rule out a small effect of a thermal spectrum in some of the systems.

- We have determined the intrinsic power law slope using the IRAC/*Spitzer* detections in the 3.6 μm

and 5.8 μm bands, avoiding the 8.0 μm band which might be contaminated by hot dust emission and the 4.5 μm band because of Hα contamination. We note however, that the 5.8 μm band could in principle also be affected by hot dust emission in large quantities, although our analysis indicates that the effect will be small and only lead to an underestimate of the inferred extinction. A dominant contribution to the uncertainty in the extinction curves comes from the photometric uncertainty in the 5.8 μm flux.

- Moreover, the correction for emission line contamination of the 3.6 μm band is not trivial and we have adopted an estimate of the η ratio from intermediate-redshift QSOs. A higher redshift template for more luminous QSOs would be highly desirable to constrain this ratio and its dispersion better. Fortunately, we have shown that the dependence of the inferred extinction on this η ratio is weak.

- The IRAC/*Spitzer* data used to fix the intrinsic power law were not obtained simultaneously with other broad-band data or the spectroscopic data. Therefore, variability is a concern. Fortunately, it appears that variability is not a major issue for these very luminous QSOs (because of their very large black hole masses). Moreover, any variability is stretched in time by a factor ~ 7 due to the high redshift of the targets. However, we cannot rule out variability in individual cases.

- Simple observational aspects such as thin cirrus during the spectroscopic observations, flux calibration difficulties, or slit loss corrections might also lead to overall systematic errors of order 10–30%. Such errors could lead to very significant effects in the inferred extinction signal.

- Foreground extinction in the Galaxy is fortunately small and has been corrected for. However, it is always possible that there may be extinction along the line of sight to an object, quite unrelated to the properties of the QSO. Foreground extinction along random lines of sight will be about an observed $A_V \approx 0.1$ (Ménard et al. 2010). In addition, there may be strong Mg II absorbers along the lines of sight to individual QSOs, such as that detected towards SDSS J1030+0524 at $z = 2.78$ (Simcoe et al. 2011). In fact, we might expect an overdensity of Mg II absorbers towards very luminous QSOs because of magnification due to gravitational lensing (as suggested for SDSS J1044−0125, see Shioya et al. 2002). Foreground extinction may lead to extinction interpreted as host galaxy extinction, and unusual extinction curves may arise from normal extinction curves contributing at the different redshifts, especially if the QSO extinction signal itself is weak.

6.5. *Theoretical SN extinction curves and the lack of evidence for a kink*

Despite the caveats discussed above, it does appear that there are significant extinction signals and that

these are related to the existence of dust in the QSO host galaxies.

The overall shape of the obtained extinction curves primarily depend on the grain-size distribution, i.e., curves are typically flattened for grain-size distributions biased towards large grains while specific features, such as for example the 1700–3000 Å Todini–Ferrara–Maiolino bump, depends on the prevalence of specific grain species.

The 'SN extinction curve' discussed in previous sections is based on the dust composition and grain size distribution predicted by theoretical models of dust formation in Type II SNe by Todini & Ferrara (2001) based on classical nucleation theory (Feder et al. 1966). The simplifications made include the assumption of uniform density and temperature as well as a full mixing of all elements in the SN ejecta. The predominant factors shaping the Todini–Ferrara–Maiolino curve (Maiolino et al. 2004) are small (≈ 10 Å) silicate grains (primarily forsterite Mg_2SiO_4), which cause the rise in the UV, and larger (≈ 300 Å) amorphous carbon grains. The characteristic plateau at 1700–3000 Å is ascribed to a minimum between two broad absorption features due to amorphous carbon and a contribution from magnetite (Fe_3O_4) (Maiolino et al. 2004). Bianchi & Schneider (2007) modified the Todini & Ferrara (2001) dust formation model and included a simple analysis of dust reprocessing due to a reverse shock penetrating the SN ejecta. This led to a shift of the grain size distribution to smaller grains (dominated by magnetite), however, maintaining the characteristic kink mentioned above, as well as the UV upturn below 1700 Å.

In the SN models for mixed and unmixed ejecta of Nozawa et al. (2003), who treat several physical process in more detail, non-carbon bearing dust is preferentially produced, with all components having grain-size distributions extending to larger grains than predicted by Todini & Ferrara (2001). Consequently, Hirashita et al. (2005) predict rather featureless extinction curves for SN dust based on these models. Extinction curves from the mixed model show a steep rise in the UV whereas extinction curves from the unmixed model are shallower. Using the same dust formation model but considering the change of the grain-size distribution due to the reverse shock (Nozawa et al. 2007) flattens the UV slope (Hirashita et al. 2008) as a consequence of efficient destruction of small grains. Such featureless, more shallow extinction curves were favoured by G10, as well as by Kawara et al. (2011) and Shimizu et al. (2011) in $z \sim 1$ ultraluminous infrared galaxies.

A common drawback of predicted SN dust extinction curves is that they are precariously dependent on the SN dust formation models used (for a detailed review of SN dust models, see Gall et al. 2011c). The models comprise different assumptions and simplifications about complex physical processes of the SN evolution and dust formation leading to different results of dust grain properties. The size distribution is also very sensitive to the number of nucleation sites; more dust seeds will lead to smaller grains. Finally, the extinction properties are usually derived by using standard Mie (1908) theory for spherical grains.

For example, Bianchi & Schneider (2007) and Fallest et al. (2011) have shown that the grain-size distribution in the dust-formation models sensitively depends on the assumed sticking probability, which is uncertain and commonly adopted to be unity. The sticking probability reflects the fraction of the colliding condensible material which will stick together, subsequently building up macroscopic dust particles. Therefore, a larger sticking probability results in larger grains. Moreover, Fallest et al. (2011) show that aspherical carbon grains tend to be larger.

Finally, we note that none of the above predictions include the effects of the likely subsequent rapid reprocessing of dust in the interstellar medium of SN-rich galaxies (e.g., Jones & Nuth 2011; Draine 2009; Michałowski et al. 2010a; Hirashita & Kuo 2011; Hirashita 2012; Asano et al. 2013).

In this paper we have obtained the first non-parametric extinction curves for dust in high-redshift QSOs. No strong evidence for unusual extinction curves, such as that proposed by Maiolino et al. (2004), was found. This suggests that the overall dust properties at low and high redshift may be quite similar. We stress however that lack of a kink or other tell-tale extinction features do not preclude SNe from being dominant sources of dust in these systems. Given the strong sensitivity to detailed SN physics and unknown dust microphysics we should continue to seek model independent observational evidence for SN extinction.

REFERENCES

Asano, R. S., Takeuchi, T. T., Hirashita, H., & Nozawa, T. 2013, arXiv:1303.5528

Bertoldi, F., Carilli, C. L., Cox, P., Fan, X., Strauss, M. A., Beelen, A., Omont, A., & Zylka, R. 2003, A&A, 406, L55

Bianchi, S., & Schneider, R. 2007, MNRAS, 378, 973

Cardelli, J. A., Clayton, G. C., & Mathis, J. S. 1989, ApJ, 345, 245

Davis, S. W., Woo, J.-H., & Blaes, O. M. 2007, ApJ, 668, 682

Demleitner, M., Accomazzi, A., Eichhorn, G., Grant, C. S., Kurtz, M. J., & Murray, S. S. 2001, in Astronomical Society of the Pacific Conference Series, Vol. 238, Astronomical Data Analysis Software and Systems X, ed. F. R. Harnden, Jr., F. A. Primini, & H. E. Payne, 321

Djorgovski, S. G., Castro, S., Stern, D., & Mahabal, A. A. 2001, ApJ, 560, L5

D'Odorico, S., et al. 2006, in Society of Photo-Optical Instrumentation Engineers (SPIE) Conference Series, Vol. 6269, Society of Photo-Optical Instrumentation Engineers (SPIE) Conference Series

Draine, B. T. 2009, in Astronomical Society of the Pacific Conference Series, Vol. 414, Cosmic Dust - Near and Far, ed. T. Henning, E. Grün, & J. Steinacker, 453

Dunne, L., et al. 2009, MNRAS, 394, 1307

Dwek, E., Galliano, F., & Jones, A. P. 2007, ApJ, 662, 927

Elíasdóttir, Á., Hjorth, J., Toft, S., Burud, I., & Paraficz, D. 2006, ApJS, 166, 443

Falco, E. E., et al. 1999, ApJ, 523, 617

Fallest, D. W., Nozawa, T., Nomoto, K., Umeda, H., Maeda, K., Kozasa, T., & Lazzati, D. 2011, MNRAS, 418, 571

Fan, X., et al. 2000, AJ, 120, 1167

—. 2001, AJ, 122, 2833

—. 2003, AJ, 125, 1649

—. 2006, AJ, 132, 117
Farrah, D., Priddey, R., Wilman, R., Haehnelt, M., & McMahon, R. 2004, ApJ, 611, L13
Feder, J., Russell, K. C., Lothe, J., & Pound, G. M. 1966, Advances in Physics, 15, 111
Fitzpatrick, E. L., & Massa, D. 2007, ApJ, 663, 320
Frank, J., King, A., & Raine, D. 1992, Accretion power in astrophysics.
Freudling, W., Corbin, M. R., & Korista, K. T. 2003, ApJ, 587, L67
Gall, C., Andersen, A. C., & Hjorth, J. 2011a, A&A, 528, A13
—. 2011b, A&A, 528, A14
Gall, C., Hjorth, J., & Andersen, A. C. 2011c, A&A Rev., 19, 43
Gallerani, S., et al. 2010, A&A, 523, A85
Gonzalo Diaz, C., Ryan-Weber, E. V., Cooke, J., Pettini, M., & Madau, P. 2011, arXiv:1104.4194
Goodrich, R. W., et al. 2001, ApJ, 561, L23
Gordon, K. D., Clayton, G. C., Misselt, K. A., Landolt, A. U., & Wolff, M. J. 2003, ApJ, 594, 279
Hirashita, H. 2012, MNRAS, 422, 1263
Hirashita, H., & Kuo, T.-M. 2011, MNRAS, 416, 1340
Hirashita, H., Nozawa, T., Kozasa, T., Ishii, T. T., & Takeuchi, T. T. 2005, MNRAS, 357, 1077
Hirashita, H., Nozawa, T., Takeuchi, T. T., & Kozasa, T. 2008, MNRAS, 384, 1725
Horne, K. 1986, PASP, 98, 609
Iwamuro, F., Kimura, M., Eto, S., Maihara, T., Motohara, K., Yoshii, Y., & Doi, M. 2004, ApJ, 614, 69
Jang, M., Im, M., Lee, I., Urata, Y., Huang, K., Hirashita, H., Fan, X., & Jiang, L. 2011, ApJ, 741, L20
Jaunsen, A. O., & Hjorth, J. 1997, A&A, 317, L39
Jiang, L., Fan, X., Vestergaard, M., Kurk, J. D., Walter, F., Kelly, B. C., & Strauss, M. A. 2007, AJ, 134, 1150
Jiang, L., et al. 2006, AJ, 132, 2127
—. 2010, Nature, 464, 380
Jones, A. P., & Nuth, J. A. 2011, A&A, 530, A44
Kawara, K., et al. 2011, MNRAS, 412, 1070
Kishimoto, M., Antonucci, R., Blaes, O., Lawrence, A., Boisson, C., Albrecht, M., & Leipski, C. 2008, Nature, 454, 492
Lawrence, A. 2012, MNRAS, 423, 451
Maiolino, R., Mannucci, F., Baffa, C., Gennari, S., & Oliva, E. 2001, A&A, 372, L5
Maiolino, R., Schneider, R., Oliva, E., Bianchi, S., Ferrara, A., Mannucci, F., Pedani, M., & Roca Sogorb, M. 2004, Nature, 431, 533
Matsuura, M., et al. 2011, Science, 333, 1258
Ménard, B., Scranton, R., Fukugita, M., & Richards, G. 2010, MNRAS, 405, 1025
Michałowski, M. J., Murphy, E. J., Hjorth, J., Watson, D., Gall, C., & Dunlop, J. S. 2010a, A&A, 522, A15
Michałowski, M. J., Watson, D., & Hjorth, J. 2010b, ApJ, 712, 942
Mie, G. 1908, Annalen der Physik, 330, 377
Motta, V., et al. 2002, ApJ, 574, 719
Nozawa, T., Kozasa, T., Habe, A., Dwek, E., Umeda, H., Tominaga, N., Maeda, K., & Nomoto, K. 2007, ApJ, 666, 955
Nozawa, T., Kozasa, T., Umeda, H., Maeda, K., & Nomoto, K. 2003, ApJ, 598, 785
Pereyra, N. A., Vanden Berk, D. E., Turnshek, D. A., Hillier, D. J., Wilhite, B. C., Kron, R. G., Schneider, D. P., & Brinkmann, J. 2006, ApJ, 642, 87
Perley, D. A., et al. 2010, MNRAS, 406, 2473
Priddey, R. S., Isaak, K. G., McMahon, R. G., Robson, E. I., & Pearson, C. P. 2003, MNRAS, 344, L74
Priddey, R. S., Ivison, R. J., & Isaak, K. G. 2008, MNRAS, 383, 289
Reichard, T. A., et al. 2003, AJ, 126, 2594
Robson, I., Priddey, R. S., Isaak, K. G., & McMahon, R. G. 2004, MNRAS, 351, L29
Schlegel, D. J., Finkbeiner, D. P., & Davis, M. 1998, ApJ, 500, 525
Shakura, N. I., & Sunyaev, R. A. 1973, A&A, 24, 337
Shang, Z., Wills, B. J., Wills, D., & Brotherton, M. S. 2007, AJ, 134, 294
Shang, Z., et al. 2005, ApJ, 619, 41
Shields, G. A. 1978, Nature, 272, 706
Shimizu, T., Kawara, K., Sameshima, H., Ienaka, N., Nozawa, T., & Kozasa, T. 2011, MNRAS, 418, 625
Shioya, Y., et al. 2002, PASJ, 54, 975
Simcoe, R. A., et al. 2011, ApJ, 743, 21
Stratta, G., Gallerani, S., & Maiolino, R. 2011, A&A, 532, A45
Stratta, G., Maiolino, R., Fiore, F., & D'Elia, V. 2007, ApJ, 661, L9
Telfer, R. C., Zheng, W., Kriss, G. A., & Davidsen, A. F. 2002, ApJ, 565, 773
Todini, P., & Ferrara, A. 2001, MNRAS, 325, 726
Toft, S., Hjorth, J., & Burud, I. 2000, A&A, 357, 115
Vacca, W. D., Cushing, M. C., & Rayner, J. T. 2003, PASP, 115, 389
Vanden Berk, D. E., et al. 2001, AJ, 122, 549
Vernet, J., et al. 2011, A&A, 536, A105
Wang, R., et al. 2010, ApJ, 714, 699
—. 2013, arXiv:1302.4154
Wyithe, J. S. B. 2004, MNRAS, 351, 1266
Zafar, T., Watson, D. J., Malesani, D., Vreeswijk, P. M., Fynbo, J. P. U., Hjorth, J., Levan, A. J., & Michałowski, M. J. 2010, A&A, 515, A94